

# A randomized benchmarking suite for mid-circuit measurements

L. C. G. Govia,\* P. Jurcevic, S. T. Merkel, and D. C. McKay  
*IBM Quantum, IBM T. J. Watson Research Center, Yorktown Heights, NY 10598, USA*

Mid-circuit measurements are a key component in many quantum information computing protocols, including quantum error correction, fault-tolerant logical operations, and measurement based quantum computing. As such, techniques to quickly and efficiently characterize or benchmark their performance are of great interest. Beyond the measured qubit, it is also relevant to determine what, if any, impact mid-circuit measurement has on adjacent, unmeasured, spectator qubits. Here, we present a mid-circuit measurement benchmarking suite developed from the ubiquitous paradigm of randomized benchmarking. We show how our benchmarking suite can be used to both detect as well as quantify errors on both measured and spectator qubits. We demonstrate the scalability of our suite by simultaneously characterizing mid-circuit measurement on multiple qubits from an IBM Quantum Falcon device, and support our experimental results with numerical simulations.

## I. INTRODUCTION

Steady progress towards quantum error correction and fault tolerant quantum computing has in recent years begun to produce experimental demonstrations of small quantum error correcting codes [1–10]. Key to most implementations of quantum error correction is the ability to repeatedly measure stabilizers of the code, often achieved via a stabilizer check circuit that encodes the outcome of the stabilizer measurement into the state of an ancilla qubit. Whether via an ancilla or measured directly [11, 12], stabilizer checks require fast and accurate mid-circuit measurement. Thus, characterizing and benchmarking mid-circuit measurement is a key capability for the development and execution of fault tolerant quantum computing.

Going beyond the typically measured state-assignment fidelity, quantum detector tomography [13–17] can be used to characterize terminal measurements in terms of a positive operator-valued measure (POVM). However, mid-circuit measurements require a quantum process tomography approach that characterizes the full quantum channel implemented by measurement [18–20]. While one can imagine extensions of these protocols to small stabilizer check circuits, the exponential resource scaling of process tomography make such characterization approaches impractical to deploy for larger quantum codes. While providing less detailed information about the measurement operation, there is a need for a scalable benchmark that can quickly assess the performance of mid-circuit measurement, and how it impacts not only the measured qubit but also those qubits connected to it.

Here, we introduce the mid-circuit measurement randomized benchmarking (mcm-rb) suite as one such benchmark. Building off the well-studied family of randomized benchmarking (RB) protocols [21–37], the mcm-rb suite comprises a central protocol, `mcm-rb`, that interleaves measurements of an ancilla qubit between the gates of Clifford RB performed on a distinct control

qubit. While writing this manuscript, we became aware of Ref. [38], which demonstrates the `mcm-rb` protocol on a trapped ion system to study the impact of both mid-circuit measurement and reset.

The two other protocols of our suite are control experiments that replace either the measurement (`delay-rb`) or the Clifford gates (`mcm-rep`) with delays of equal time duration to the replaced operation. Comparison between the decay curves of `mcm-rb` with the control experiments allow for the identification, and in some cases quantification, of the error induced by measurement on the control and ancilla qubits under the standard RB assumptions (i.e. Markovianity [22]). By the addition of these protocols, and the quantification of measurement-induced error that they allow, our mcm-rb suite extends the work of Ref. [38] into more general purpose benchmarking.

This manuscript is organized as follows. In section II we describe the procedure of the mcm-rb suite, and in section III we discuss a classification of errors that the suite can detect. In section IV we demonstrate the mcm-rb suite on an IBM Quantum device, and in section V we present supporting numerical simulations. Finally, in section VI we discuss a limitation and potential extension of the protocol, and in section VII we make our concluding remarks. Further details of our experimental and numerical results can be found in the Appendices.

## II. MID-CIRCUIT MEASUREMENT RANDOMIZED BENCHMARKING SUITE

The mcm-rb suite is defined by the set of RB-style protocols (`mcm-rb`, `delay-rb`, `mcm-rep`), for which example circuits are shown in Fig. 1. The first protocol, `mcm-rb`, interleaves ancilla-qubit mid-circuit measurements between Clifford gates performed on the control qubit. Similar to simultaneous RB [26], it performs a single-subsystem twirl on the potentially two-qubit error induced by ancilla measurement. The second protocol, `delay-rb`, is analogous to interleaved RB (IRB) [25] on the control qubit, with the interleaved gate a noisy identity corresponding to a delay of equal duration to the ancilla-qubit measurement.

\* [lcggovia@ibm.com](mailto:lcggovia@ibm.com)

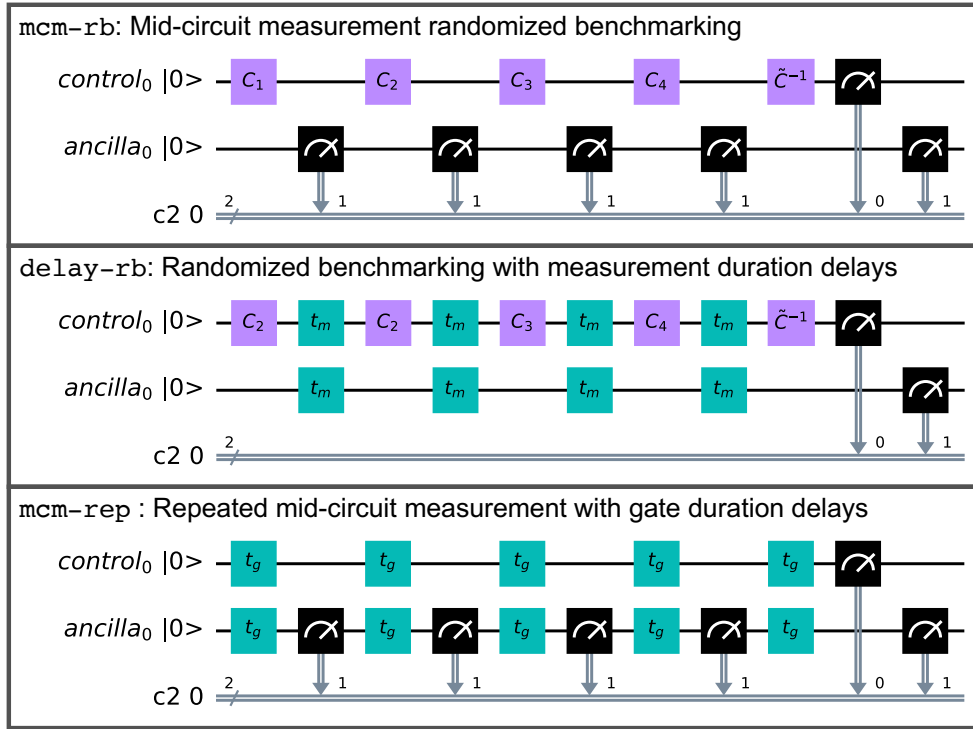


FIG. 1. **Example circuits of the mcm-rb suite protocols.** Sequence length  $N_i = 4$  for all three protocols. (Upper panel) **mcm-rb** circuit with Clifford gates on the control qubit interleaved by measurements on the ancilla. (Middle panel) **delay-rb** circuit where Clifford gates on the control qubit are interleaved with delays of duration  $t_m$ , the length of an ancilla measurement. (Lower panel) **mcm-rep** with repeated measurements on the ancilla qubit interleaved by delays of duration  $t_g$ , the length of a control qubit Clifford gate.

Together, these two protocols form an IRB procedure designed to detect errors on the control qubit induced by the ancilla-qubit measurement. Though it contains an interleaved gate itself, **delay-rb** is the reference sequence, and **mcm-rb** is the interleaved error sequence. It is important to reference **mcm-rb** by a sequence that contains interleaved delays in order to remove the trivial  $T_1$  and  $T_2$  decay of the control qubit during the potentially long measurement time, as this error may otherwise dominate other errors induced by the ancilla-qubit measurement.

The final protocol, **mcm-rep**, is included to detect errors on the ancilla due to its own measurement, and is a modification of quantum non-demolition tests, e.g. Ref. [7]. Delays of equal duration to the control-qubit Clifford gates are interleaved between repeated measurements to keep all three protocols of equal duration (for a given sequence length), and to detect measurement and logical basis misalignment. We discuss the latter point in more detail in section IV. Comparing **mcm-rep** to **mcm-rb** is also useful for detecting certain kinds of two-qubit errors that require one qubit to be excited, of which we show an example in sections IV and V.

The mcm-rb suite is implemented similar to any RB-style protocol. A set of sequence lengths,  $\{N_i\}_i$ , is chosen, and for **mcm-rb** and **delay-rb** each sequence of length  $N_i$  consists of  $N_i$  random single-qubit Clifford

gates on the control qubit interleaved by either measurements on the ancilla, or delays of equal duration, respectively. A final Clifford gate that is meant to invert the action of the previous  $N_i$  Cliffords terminates every circuit. At each sequence length, many random Clifford circuits are executed. For **mcm-rep** the circuit consists of  $N_i$  ancilla measurements interleaved by delays of equal duration to the control qubit Clifford gates. In this manuscript we have chosen  $N_{\max} = 150$ .

For all three protocols, the outcomes of the mid-circuit measurements are discarded, and the ground state probability at the end of each circuit is estimated from the terminal measurement. This probability is averaged over the random Clifford circuits and its decay as a function of sequence length is fit to the exponential function  $P_0 = A\alpha^{N_i} + B$ . The RB-decay parameter  $\alpha$  defines the error per Clifford/measurement for each qubit by  $\text{EPC/M} = (1 - \alpha)/2$ , while the other fit parameters  $A$  and  $B$  account for system preparation and measurement error (SPAM).

As we demonstrate in our experimental results of section IV, the mcm-rb suite can be applied simultaneously to multiple control and ancilla qubits. This can be used to test the impact of measurement of a central ancilla on multiple control qubits, or to test the impact of the measurement of multiple ancilla qubits on a single control.

Error Signature	EPC/M
No measurement induced error	$\epsilon_{\nu}^a \approx 0 \forall \nu$ $\epsilon_{\nu}^c \approx \epsilon_{\text{del}}^c, \epsilon_{\text{rep}}^c \approx 0$
Non-QND measurement error	$\epsilon_{\text{del}}^a \approx 0, \epsilon_{\text{rb}}^a > 0, \epsilon_{\text{rep}}^a > 0$ $\epsilon_{\nu}^c \approx \epsilon_{\text{del}}^c, \epsilon_{\text{rep}}^c \approx 0$
Measurement induced control error	$\epsilon_{\nu}^a \approx 0 \forall \nu$ $\epsilon_{\nu}^c > \epsilon_{\text{del}}^c, \epsilon_{\text{rep}}^c \geq 0$
Measurement induced 2-qubit error	$\epsilon_{\text{del}}^a \approx 0, \epsilon_{\text{rb}}^a \geq 0, \epsilon_{\text{rep}}^a \geq 0$ $\epsilon_{\nu}^c > \epsilon_{\text{del}}^c, \epsilon_{\text{rep}}^c \geq 0$
RB cross-talk error	$\epsilon_{\text{rep}}^a \approx 0, \epsilon_{\text{rb}}^a > 0, \epsilon_{\text{del}}^a > 0$ $\epsilon_{\nu}^c \approx \epsilon_{\text{del}}^c, \epsilon_{\text{rep}}^c \approx 0$

TABLE I. Error signatures detected by the mcm-rb suite that we consider in this paper. For each error signature, the expected relationships between the EPCs and EPMS are shown. Each  $\epsilon_{\nu}^q$  is an EPC/M with  $q \in \{c, a\}$  for control and ancilla, and  $\nu \in \{\text{rb}, \text{del}, \text{rep}\}$  for **mcm-rb**, **delay-rb**, and **mcm-rep**.

We study both applications in this work, as we simultaneously perform the mcm-rb suite across control and ancilla qubits on our device. While simultaneous Clifford gates on control qubits could introduce cross-talk error, since both **mcm-rb** and **delay-rb** would be performed with simultaneous gates, we can still use **delay-rb** as the reference sequence to quantify the error induced by measurement in **mcm-rb**.

### III. ERROR DETECTION WITH MID-CIRCUIT MEASUREMENT RB

In this section we demonstrate the capability of the mcm-rb suite (**mcm-rb**, **delay-rb**, **mcm-rep**) to detect, and in many case estimate the magnitude of, errors induced by mid-circuit measurement on either the control or (measured) ancilla qubit. To do so, rather than focus on the effects of specific errors, we classify the distinct *error signatures* that the mcm-rb suite's decay curves can exhibit, where each error signature can have more than one possible underlying physical error mechanism.

Error signatures are classified by the comparing the error per Clifford (EPC) of the control and error per measurement (EPM) of the ancilla for the three components of the mcm-rb suite. From here one, we denote the EPC and EPM by  $\epsilon_{\nu}^q$ , with  $q \in \{c, a\}$  for control and ancilla respectively, and  $\nu \in \{\text{rb}, \text{del}, \text{rep}\}$  for **mcm-rb**, **delay-rb**, and **mcm-rep** respectively. Table I outlines the error signatures we consider, and the expected relationships between the various EPCs and EPMS.

It should be noted that multiple physical errors which result in distinct error signatures can occur simultaneously, such that the decay curves of the mcm-rb suite display a combination of the error signatures listed in Table I. In this case, one has to determine the likely underlying error signatures through a process of elimination given which  $\epsilon_{\nu}^q$  are nonzero. While it is impossible to distinguish some combinations, e.g. a non-QND measurement and either a measurement induced control or

two-qubit error, there is sufficient information given by the mcm-rb suite to use either in a debugging cycle or to use with knowledge of the device physics to determine the likely error signatures and their underlying causes.

An important question is whether or not the mcm-rb suite can *quantify* the EPM or the added EPC due to mid-circuit measurement. Since we measure the EPM by exponential fit, to quantify the error due to mid-circuit measurement on the measured ancilla we require that the error process induce an exponential decay of ground-state probability with sequence length  $\ell$ . While this is not generically guaranteed, we argue in the following non-QND error subsection that it applies to a wide class of error models in the small error limit.

As for quantifying the added EPC due to mid-circuit measurement, as mentioned previously from the control qubit's perspective the pair of experiments **mcm-rb** and **delay-rb** together form an interleaved RB (IRB) protocol. **mcm-rb** interleaves a noisy identity operation on the control qubit, with the error induced by mid-circuit measurement on the ancilla. Thus, if the measurement induced error satisfies the necessary assumptions of IRB [25] we can quantify the error due to mid-circuit measurement as we would for any IRB procedure. We note that as with any IRB estimate of the added error, one must exercise caution with respect to quantitative accuracy as the accuracy of IRB estimates is very sensitive to the underlying errors of the reference sequence (in our case **delay-rb**), as well as the nature of the interleaved error.

### IV. MCM-RB IN EXPERIMENT

In this section, we demonstrate the practical application of the mcm-rb suite on the IBM Quantum Falcon R8 device **ibm\_peekskill**. Where possible, we present an example of each error signature from Table I using mcm-rb data taken on **ibm\_peekskill**. To showcase the scalability of simultaneous mcm-rb, the mcm-rb suite experiments were performed in parallel on 5 ancilla-control qubit sets for a total of 17 qubits operating simultaneously. Two distinct 17-qubit configurations on **ibm\_peekskill** were considered, such that 23 of the 27 qubits on **ibm\_peekskill** were studied. For further details see Appendix A, and for complete mcm-rb suite data on all 23 qubits see Appendix C.

#### A. No Measurement Induced Error

The trivial error signature occurs when the EPC for **mcm-rb** and **delay-rb** are indistinguishable from one another, the EPC is zero for **mcm-rep**, and the EPM is zero for all three experiments in the mcm-rb suite. In this case, interleaving mid-circuit measurements has no effect on either the control or ancilla qubit, which is the desired outcome for most applications. An example of no mea-

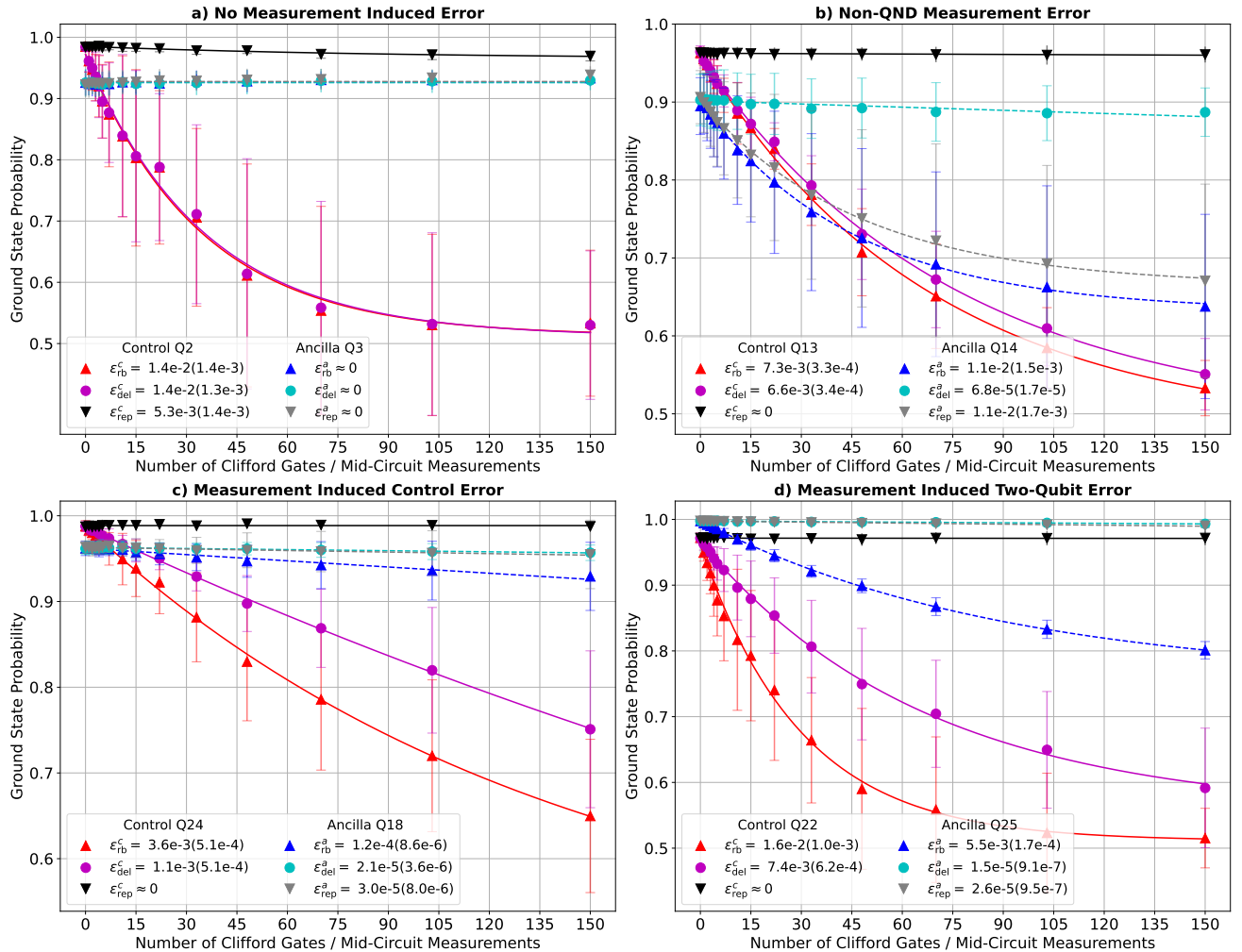


FIG. 2. Error signatures of the mcm-suite on `ibm_peekskill`. For each curve, markers and error bars show the mean and one standard deviation respectively of the ground state probability over 40 random RB sequences. **a) No measurement induced error** on Q17 and Q18. Even though ancilla Q18 has low readout fidelity, the mcm-rb suite shows no impact of mid-circuit measurement on either control or ancilla. **b) Non-QND measurement error** for Q13 and Q14. The control Q13 is mostly unaffected by mid-circuit measurement, but the ancilla Q14 state decays with or without Clifford RB on the control. **c) Measurement induced control error** for Q15 and Q12. Decay of the control Q15 is greatly enhanced by mid-circuit measurement, but the ancilla Q12 is unaffected. **d) Measurement induced 2-qubit error** for Q22 and Q25. For this, which we believe is a measurement induced collision, the decay of the control Q22 is greatly enhanced by mid-circuit measurement, and the ancilla Q25 decays only for the `mcm-rb` protocol.

surement induced error from `ibm_peekskill` is shown in Fig. 2a). This pair of qubits was specifically chosen to also highlight that non-unity readout fidelity on the ancilla qubit does not impact the mcm-rb suite.

## B. non-QND Measurement

A quantum non-demolition (QND) measurement is one for which the measurement operator commutes with the system Hamiltonian, and leaves the system in the logical eigenstate corresponding to the reported measurement outcome [39]. As such, non-QND measurement is commonly used as a catch-all term to describe any error that

changes the state of the system from that reported. One example is an error process that has a finite probability of flipping the state of the qubit after measurement.

However, measurements that project the system onto an eigenbasis that is not the logical basis, i.e. the logical and measurement bases are misaligned, are also non-QND. A protocol based on repeated measurements with no delays can detect non-QND errors such as measurement-induced state flips [7], but will be insensitive to errors due to logical and measurement basis misalignment. This insensitivity is due to the fact that from the measurement's perspective misalignment errors are not an error, and repeated measurement with no delay will repeatedly project the system into the same mea-

surement basis state, with no probability of a state flip.

On the other hand, as `mcm-rb` and `mcm-rep` have delays on the ancilla between repeated measurements to accommodate control Clifford gates, there is time for the ancilla logical Hamiltonian to evolve the system out of a measurement basis state. This results in a finite probability of a measurement basis state flip, and thus nonzero  $\epsilon_{rb}^a$  and  $\epsilon_{rep}^a$ , such that the `mcm-rb` suite can detect both kinds of non-QND error. Nevertheless, in our experimental system the mid-circuit measurements have been tuned up to mitigate the impact of Stark shifts and dephasing due to residual photons in the measurement resonator [40]. This removes a major source of misalignment errors present in our system [41], though others may still persist [42].

For a generic non-QND error, as there is no unitary twirl applied to the ancilla qubit we cannot guarantee exponential decay of its ground-state probability. As a result, the EPM estimated by an exponential fit may not be a faithful quantifier of the true EPM. However, in the appropriate limit exponential decay can be obtained for non-QND error models that result in the same probability of a state flip after each measurement. Such error models are common, e.g. arising due to spurious qubit transitions driven by the measurement pulse, or the action of the logical Hamiltonian during the delay time between measurements with a misaligned logical and measurement bases.

If the probability of a state flip after each measurement is  $p$ , then for an `mcm-rb` and `mcm-rep` sequence of length  $N$  the ground state probability for the terminal measurement is the probability of an even number of state flips during the sequence, which is given by

$$P_{GS} = \frac{(1-p)^{N+2} - p^{N+2-w}(1-p)^w}{1-2p} \quad (1)$$

with  $w = 0$  for even  $N$  and  $w = 1$  for odd  $N$ . In the limit of a small error such that  $p \ll 1$  this becomes approximately a single exponential decay with  $P_{GS} \propto (1-p)^N$ . When this is the case, an exponential fit to the data allows us to quantify the amount of induced error per measurement.

An example of a non-QND measurement error signature from `ibm_peekskill` is shown in Fig. 2b). The ancilla decay clearly shows the tell-tale signature of a non-QND error:  $\epsilon_{rb}^a \approx \epsilon_{rep}^a > 0$ , and we note that these decay curves are well fit by an exponential. While there is weak decay of the ancilla for long `delay-rb` sequences, with  $\epsilon_{del}^a \neq 0$ , this is three orders of magnitude less than  $\epsilon_{rb}^a$ , such that it is clear the measurement is negatively impacting the ancilla. The control EPCs with and without mid-circuit measurements are not indistinguishable, indicating that there may also be some measurement induced error on the control qubit for this qubit pair.

### C. Measurement Induced Control Error

The `mcm-rb` suite was designed to detect any errors induced by the measurement on the control qubit, and this error signature is indicative of an induced error that impacts *only* the control qubit, such that the ancilla qubit can be ignored as it is unaffected. This error signature can be understood as an additional error interleaved between the non-ideal Clifford gates on the control qubit. Assuming the usual requirements of IRB hold for the measurement induced error [25], e.g. it is Markovian and at most weakly gate dependent, then the standard IRB procedure can be used to compare the decay of the `mcm-rb` and `delay-rb` experiments to quantify the error induced on the control qubit by mid-circuit measurement. Note that it is important to use `delay-rb` as the reference sequence to capture the control-error due to interleaving a long delay between Clifford gates, and the magnitude of this delay error can be quantified using IRB comparing `delay-rb` to a standard RB experiment with no delay.

An example of a measurement induced control error signature from `ibm_peekskill` is shown in Fig. 2c). For the control qubit EPCs,  $\epsilon_{rb}^c$  is more than a factor of three larger than  $\epsilon_{del}^c$ , indicating a significant impact of mid-circuit measurement on the control qubit. The EPMs for the ancilla qubit are all almost negligible, except for  $\epsilon_{rb}^a$ , which indicates there may also be evidence for a weak two-qubit measurement induced error or RB cross-talk error.

While the physical origin of this error cannot be determined with certainty, given the nature of the hardware platform and the fact that  $\epsilon_{rep}^c \approx 0$ , it is likely due to either a measurement induced Stark shift, or weak cross-dephasing on the control qubit. The power of the `mcm-rb` suite is that it can quickly identify all such issues across an entire chip, which can then be explored in more detail with slower techniques to determine their origin.

### D. Measurement Induced Two-Qubit Error

Unlike the error signatures we have thus far considered, there are sufficiently diverse measurement induced two-qubit errors that they will not all result in the same error signature. We do expect that any measurement induced two-qubit error will result in a faster decay of the control qubit for `mcm-rb` compared to `delay-rb`. Unfortunately, the control `mcm-rb` decay is not guaranteed to be exponential as only the control-qubit is twirled. However, from the simultaneous RB protocol [26] we know that in the limit of small two-qubit error the decay of a single-subsystem Clifford twirl will still be approximately exponential, such that we can again quantify the added error on the control using an IRB procedure comparing `mcm-rb` and `delay-rb`.

The ancilla may decay for `mcm-rb`, but one can imagine error models where this would not be the case. For

instance, if the measurement induced error flipped the state of the control conditioned on the ancilla being in its ground state (in terms of a circuit this is a CNOT sandwiched by  $X$ -gates on the ancilla) then this would have no effect on the ancilla. Note that, i) this is a true two-qubit error, only because the ancilla stays in the ground state for the entire protocol do we see that it is entangling; and ii) this error model with the control and ancilla roles reversed would result in decay for both qubits due to the Clifford twirl on the control. Similarly, either the control, ancilla, both, or neither may decay for `mcm-rb`. This depends on whether or not the Clifford gates on the control are needed to detect the specific kind of error induced by mid-circuit measurement.

An example of a measurement induced two-qubit error signature from `ibm_peekskill` is shown in Fig. 2d). In this case, it is clear that this is a two-qubit error as we have that both a substantial  $\epsilon_{rb}^a > 0$  and  $\epsilon_{rb}^c > \epsilon_{del}^c$ , with all three decay curves well fit by exponential functions. For this particular two-qubit error,  $\epsilon_{rb}^{a/c}$  is negligible compared to  $\epsilon_{rb}^a$ . As we explain in more detail with a numerical simulation model in Section V, we attribute this particular kind of two-qubit error signature to a measurement induced collision. The ancilla qubit is Stark-shifted by the photons in the measurement cavity to a frequency close enough to the control qubit such that near-resonant excitation exchange can occur. The tell-tale signature that this is likely a collision is the fact that  $\epsilon_{rb}^a \gg \epsilon_{rep}^a$ , indicating that for a control qubit in its ground state the ancilla is not impacted.

### E. RB Cross-talk

Finally, we briefly discuss an error signature detectable by the `mcm-rb` suite, but which has nothing to do with mid-circuit measurement. If the implementation of the Clifford gates on the control qubit impacts the ancilla qubit, i.e. if there is cross-talk between the qubits for single qubit gates, then the `mcm-rb` and `delay-rb` curves for the ancilla will likely decay. However, due to the lack of a Clifford twirl on the ancilla, the `mcm-rb` suite cannot say much quantitatively about this error. By design the `mcm-rb` suite is meant to benchmark errors induced by measurement on the control qubit(s), and other protocols exist to benchmark [26, 35] or characterize [43] cross-talk.

## V. NUMERICAL SIMULATION OF MCM-RB

In the following subsections, for each non-trivial error signature of Table I we use numerical simulation to study example physical error mechanisms that lead to the error signature. Our simulations are performed using the quantum circuit simulator in Qiskit Aer [44], which natively supports error processes such as the depolarizing channel and decoherence generated by qubit  $T_1$  decay

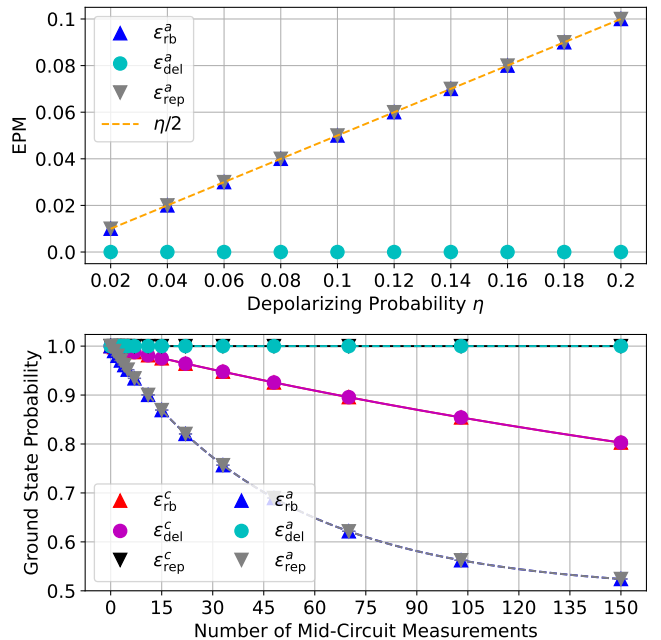


FIG. 3. **Non-QND Measurement Simulations.** (Upper panel) EPM for the ancilla qubit for the three `mcm-rb` suite experiments. The EPM for `mcm-rb` and `mcm-rep` accurately estimate the simulated EPM of  $\eta/2$ , shown in the dashed orange line. (Lower panel) Example `mcm-rb` suite decay curves for a non-QND measurement error due to a depolarizing channel with depolarizing probability  $\eta = 2\%$ .

and  $T_2$  dephasing. Additionally, one can add custom error processes either as unitary gates or via their Kraus decomposition, and we make use of this functionality for several of the measurement induced errors considered in the subsequent subsections.

In addition to the measurement induced error, our simulations add depolarizing error to each single qubit gate on the control qubit, as well as an amplitude and phase damping channel to the control qubit for each ancilla measurement. The latter is equivalent to the decoherence generated by control qubit  $T_1$  and  $T_2$  decoherence during the measurement, with parameters chosen to be representative of our experimental setup. For further details see Appendix B.

### A. Non-QND Measurement

To model non-QND measurement, we take a simple approach and consider the application of a depolarizing channel after each mid-circuit measurement. A single-qubit depolarizing channel acts as

$$\mathcal{E}_{\text{dep}}(\rho) = (1 - \eta)\rho + \eta \frac{\hat{\mathbb{I}}}{2}, \quad (2)$$

with  $\eta$  the depolarizing probability. For our simulations we scan  $\eta$  from 2% to 20%, as shown in Fig. 3. The

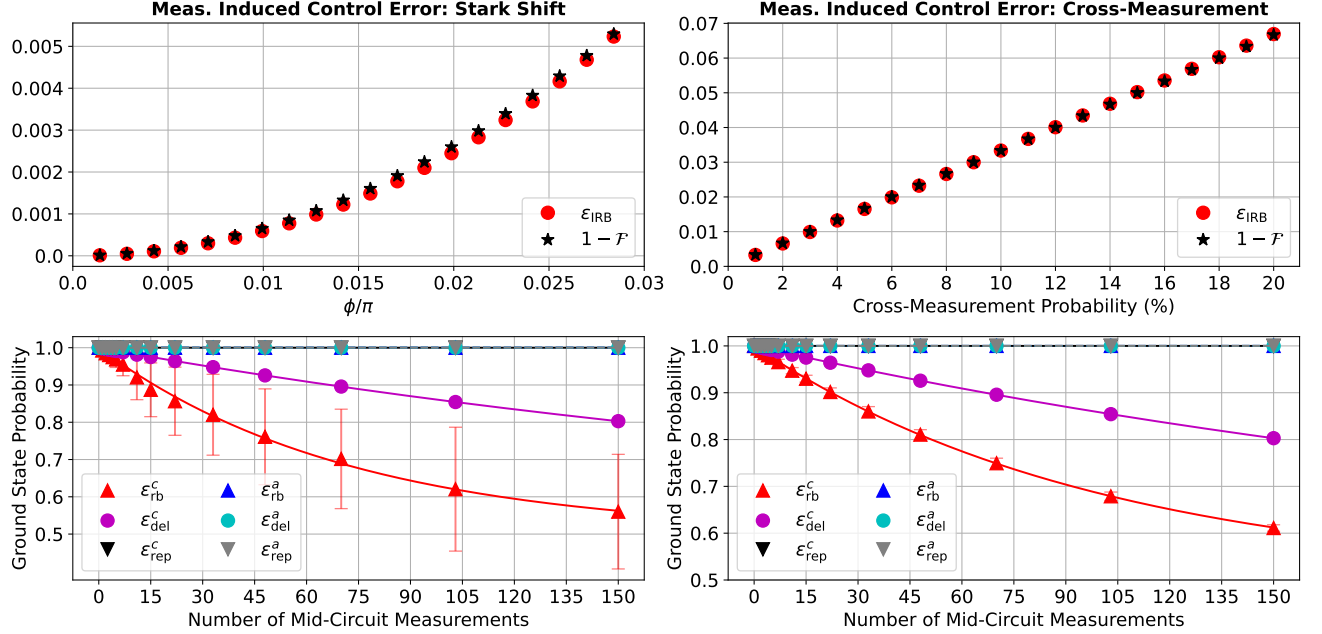


FIG. 4. **Measurement Induced Control Error.** Left column:  $Z$ -phase error due to control-qubit Stark shift. Right column: Error due to a cross-measurement on the control qubit as described by the channel of Eq. (3). The upper panels shows the added error due to measurement as estimated by IRB,  $\epsilon_{\text{IRB}}$ , compared to the average gate infidelity  $1 - \mathcal{F}$ . In both cases there is good agreement between the estimated and exact values. The lower panels show example `mcm-rb` suite decay curves, for  $\phi/\pi \approx 0.03$  and  $p_m = 0.01$ . Despite their similar decay rates, note the considerable spread in the control-qubit `mcm-rb` decay curve for the coherent error compared to the incoherent error.

lower panel shows an example of the expected `mcm-rb` suite decay curves for a non-QND measurement error, in this case for  $\eta = 2\%$ . The upper panel shows that the EPM for both `mcm-rb` and `mcm-rep` accurately estimate the simulated error per measurement, which for the depolarizing channel is  $\eta/2$ .

### B. Measurement Induced Control Error

We consider two models for physical error mechanisms that induce control qubit errors. The first is a measurement-induced Stark shift, which adds a  $Z$ -phase error to the control qubit after every measurement via the unitary  $\hat{U}_{\text{Stark}} = e^{-i\phi\hat{\sigma}_z}$ . For a cQED system such as `ibm_peekskill`, this can occur when readout photons intended for the ancilla-qubit resonator populate the control-qubit resonator. Then, via the dispersive interaction  $\hat{H} = \chi\hat{\sigma}_z^c\hat{n}$  between the control-qubit and its readout resonator, the control frequency is Stark shifted by  $2\chi\bar{n}$  during measurement, where  $\bar{n}$  is the average number of photons in the resonator. For a mid-circuit measurement of duration  $t_m$  this leads to a Stark-phase error with  $\phi = 2\chi\bar{n}t_m$ .

The second model is cross-measurement, where with some probability  $p_m$  the measurement of the ancilla also strongly measures the control qubit. This error is described by the quantum channel,  $\mathcal{E}_{p_m}^c$ , that completely

dephases the control qubit with probability  $p_m$ . The Kraus representation of this channel is given by

$$\begin{aligned} \hat{K}_0 &= \sqrt{p_m} |0\rangle\langle 0|, \quad \hat{K}_1 = \sqrt{p_m} |1\rangle\langle 1|, \\ \hat{K}_2 &= \sqrt{1 - p_m} \hat{\mathbb{I}}. \end{aligned} \quad (3)$$

In a continuous time model this error could also be described by dephasing on the control qubit during the measurement with a rate  $\gamma$  defined by  $e^{-\gamma t_m} = 1 - p_m$ . In a cQED system, this error can occur due to readout photons that leak into the control-qubit resonator, and is also possible in an ion trap system due to scattering of the readout laser pulse or photons fluoresced by the ancilla-qubit [38].

The results of our simulations are shown in Fig. 4, with the left column showing the results for the Stark shift error model and the right column for the cross-measurement error model. The lower panels show examples of the `mcm-rb` suite decay curves for these error models, and it is important to highlight that despite very different underlying physics, they produce the same error signature:  $\epsilon_{rb}^c \gg \epsilon_{del}^c$  with all other EPC/M zero. This is to be expected as they are both errors that impact only the control qubit.

The upper panels show the error induced on the control qubit per mid-circuit measurement as estimated by IRB ( $\epsilon_{\text{IRB}}$ ), and compare to the average gate infidelity, i.e.  $1 - \mathcal{F}$ , with  $\mathcal{F}$  the average gate fidelity which can be calculated exactly for these error channels. In both cases

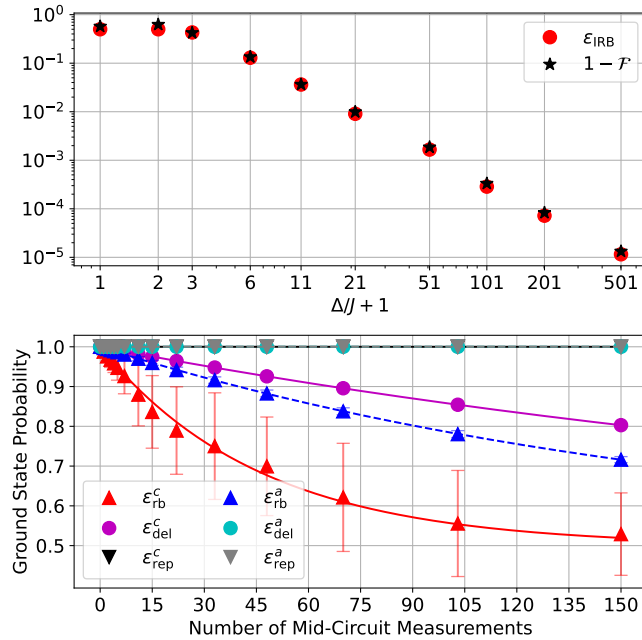


**FIG. 5. Measurement Induced Two-Qubit Error.** The measurement induced collision error model of Eq. (4) parameterized by the ratio of the detuning and coupling,  $\Delta/J$ . (Upper panel) Added error due to measurement as estimated by IRB,  $\epsilon_{\text{IRB}}$ , compared to the average gate infidelity  $1 - \mathcal{F}$ . Note that the values of the  $x$ -axis are shifted by one to accommodate the log-log scale. (Lower panel) Example mcm-rb suite decay curves for a measurement induced collision with  $\Delta/J = 20$ .

the IRB estimate is reasonably accurate, but it is noticeably less so for the coherent Stark shift error model. This highlights the caution necessary when using IRB, especially for coherent error and if a high degree of accuracy is required. Comparing the mcm-rb suite decay curves of the lower panels, it is unsurprising that the IRB estimate is less accurate for the coherent Stark-shift error, given the much larger spread in the control-qubit decay curves for mcm-rb observed for that error model.

### C. Measurement Induced Two-Qubit Error

From the broad class of possible two-qubit errors we consider one that is physically motivated by the superconducting hardware platform, and has an interesting error signature. In particular, we explore the impact of a measurement induced collision, where the measurement induced Stark shift on the ancilla qubit brings it close to resonance with the control qubit. We consider a minimal model for this system that is platform agnostic, described by a coupled control-ancilla system. The Hamiltonian describing their interaction is

$$\hat{H} = \frac{\Delta}{2} \hat{\sigma}_z^a + J (\hat{\sigma}_-^a \hat{\sigma}_+^c + \hat{\sigma}_+^a \hat{\sigma}_-^c), \quad (4)$$

where the qubits are in a frame rotating at the frequency of the control qubit such that  $\Delta = \omega_a - \omega_c$ , with  $\omega_a$  the Stark-shifted frequency of the ancilla qubit. To implement our error model in simulation, after every measurement we add the unitary error  $\hat{U}_{\text{Col}} = e^{-i\hat{H}t_m}$ , which corresponds to evolving the system for a time  $t_m$  under the evolution of the collision Hamiltonian.

Figure 5 shows the results of these simulations. As in our other simulations, the upper panel shows that the error added by measurement can be accurately estimated using an IRB procedure to compare  $\epsilon_{\text{rb}}^c$  and  $\epsilon_{\text{del}}^c$ . See Appendix B for further information on our calculation of the average gate infidelity,  $1 - \mathcal{F}$ , of the effective single qubit channel on the control qubit induced by this two-qubit error channel. We note that even though the IRB prediction is accurate, for  $\Delta/J < 5$  the decay curves are not well fit by exponential functions, as the error induced by the two-qubit channel is too large for the single-subsystem twirl that is performed [26].

The lower panel shows an example of the expected mcm-rb suite decay curves ( $\Delta/J = 20$ ), with  $\epsilon_{\text{rb}}^c \gg \epsilon_{\text{del}}^c$  and finite  $\epsilon_{\text{rb}}^a$ , all of which display exponential decay. It is the finite  $\epsilon_{\text{rb}}^a$  that distinguishes a two-qubit error from an error only on the control qubit. As it requires one qubit to be at least partially excited,  $\epsilon_{\text{rep}}^a = 0$  for a measurement induced collision, but other two-qubit error sources may have finite  $\epsilon_{\text{rep}}^a$ .

## VI. DISCUSSION

For our demonstrations of the mcm-rb suite we have exclusively focused on the scenario where the ancilla qubit is initially prepared in the ground state. An equivalent set of experiments could be performed with the ancilla qubit prepared in the excited state, and this would return different results if the effective error channel on the control qubit depends on the ancilla state. On its own this is not problematic, and one could simply repeat the mcm-rb suite for both ancilla initial states. However, if there is also an error source driving ancilla state flips, then the control-qubit error in a given sequence may become non-Markovian.

As an example, consider the experimentally relevant situation of an ancilla with relaxation characterized by a timescale  $T_1$ . If the ancilla is initialized in the excited state, then for the initial duration of an RB sequence ( $t \ll T_1$ ) the effective error channel on the control qubit is approximately static, given by the error channel conditioned on the ancilla in the excited state. For sequences with duration longer than  $T_1$ , near the end of the sequence ( $t \gg T_1$ ) the effective control-qubit error is again approximately static, but now given by the error channel conditioned on the ancilla in the ground state.

Crucially, at some point during the sequence the control-qubit error channel changes, and thus across the total sequence the control-qubit error cannot be consistently defined by one single-qubit quantum channel. The

control-qubit error is temporally correlated across the sequence in a non-trivial way, with quasi-static error that exhibits at most one switch during a given sequence. The impact of such temporal correlations on RB has been previously studied [45], and in practice it does not preclude EPC estimation, but may make the estimates less reliable and require more random sequences for convergence.

In our experimental system, the  $T_1$  time is a factor of 2 or 3 longer than the longest sequences we use in our mcm-rb experiments. Our system exhibits ancilla-state-dependent control-qubit error due to the presence of weak  $ZZ$ -coupling between many of the qubits on the device. Due to the fact that gates are calibrated with all spectator qubits in the ground state, this results in a coherent error on the control qubit only for an excited ancilla,  $\hat{U}_{ZZ} = e^{-i\hat{H}_{ZZ}t_m}$ , described by the Hamiltonian

$$\hat{H}_{ZZ} = \nu |e\rangle\langle e|_a \otimes \hat{\sigma}_z^c, \quad (5)$$

where  $\nu$  is the  $ZZ$ -coupling rate.

We simulate the impact of this error channel combined with relaxation of the ancilla-qubit on the mcm-rb protocol with the ancilla initialized in the excited state, and the results of these simulations are shown in Fig. 6. When  $T_1$  is very short (e.g. 0.1 or 1.0  $\mu$ s) the ancilla relaxes almost immediately, such that only the first gates in a given sequence experience the error  $\hat{U}_{ZZ}$ . All but the first few sequence lengths are well fit by an exponential with an  $\epsilon_{rb}^c$  calculated from the control-qubit error model for the ancilla in the ground state. For very long  $T_1$  (e.g. 100  $\mu$ s), only the longest sequences are likely to experience ancilla relaxation. Aside from small deviations at the end, the full decay curve is well fit by an exponential with  $\epsilon_{rb}^c$  calculated from  $\hat{U}_{ZZ}$ . For intermediate  $T_1$  (e.g. 10  $\mu$ s) the fit quality decreases significantly for the longer sequences where an ancilla relaxation, and thus an inconsistency in the control-qubit error, is likely to occur.

As these simulations show, the non-Markovian characteristic of the control-qubit error induced by the combination of  $ZZ$ -coupling and ancilla relaxation reduce the reliability of the EPCs obtained from RB fitting. Though our ancilla qubits have an average  $T_1 > 100 \mu$ s, to avoid the complications of temporally correlated error in RB we have focused on benchmarking mid-circuit measurement with the ancilla in the ground state.

One possible way to overcome this issue would be to randomize either the initial ancilla state preparation, or randomize state re-initialization after each mid-circuit measurement. This can be done by randomly inserting identity or  $\hat{X}$ -gates at the start of the circuit, or after each mid-circuit measurement. In aggregate, the control qubit will then experience the average error channel induced by ancilla measurement, unconditioned on the ancilla state.

Similarly, we could randomize the initialization of the control qubit, which should not impact mcm-rb or delay-rb, but could potentially change the result of mcm-rb. This would be the case, for example, if the measurement induced an amplitude damping error on the

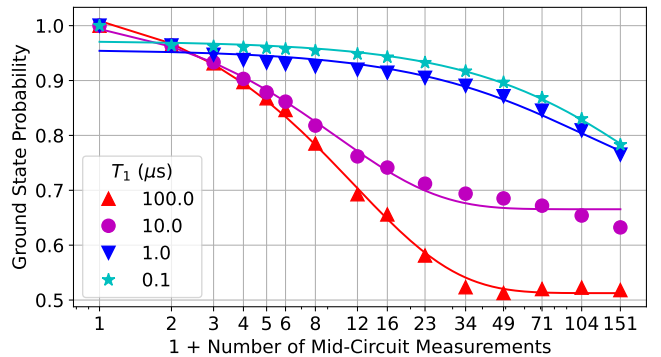


FIG. 6. **Non-Markovian Control Error Induced by the Ancilla.** Control-qubit decay of the mcm-rb protocol, i.e.  $\epsilon_{rb}^c$ , for the  $ZZ$ -coupling error model of Eq. (5) combined with ancilla relaxation decay for varying values of the relaxation timescale  $T_1$ . For all curves, the ancilla-qubit was initialized in the excited state,  $\nu = 50$  kHz, and  $t_m$  is as before. Note that the x-axis is shifted by 1 to accommodate a value of 0 on the log-scale.

control qubit. We leave exploration of these extensions of the mcm-rb suite, and how their measured EPCs connect to experimentally relevant quantities, for future study.

## VII. CONCLUSION

In this work we have presented a randomized benchmarking suite for mid-circuit measurements, whose central protocol interleaves mid-circuit measurements on an ancilla qubit between Clifford gates on a control qubit. The remaining two protocols of the suite replace either the mid-circuit measurement or the Clifford gates with idle delays of equal duration, and serve as reference experiments to enable error quantization through an interleaved randomized benchmarking procedure. As we have demonstrated on an IBM Quantum Falcon device, our benchmarking suite can be trivially extended to an entire multi-qubit chip, benchmarking multiple control and ancilla qubits simultaneously.

The mcm-rb suite classifies errors based on their error signature, which is the relationship between the RB-decay curves from the three protocols in the suite for both the control and ancilla qubits. We discussed the three major error signatures: non-QND measurement error, control-qubit error, two-qubit error; and highlighted examples of these error signatures from our deployment of the mcm-rb suite on an IBM Quantum Falcon device. Each error signature can be the result of many different physical error models, and we explored several in numerical simulation. By comparing to the average infidelity of our simulation models, we demonstrated that the mcm-rb suite can function as an IRB procedure and quantify the error added by mid-circuit measurement.

Our benchmarking suite can be readily adapted to other quantum-classical operations beyond mid-circuit

measurement. These include a larger part of or even the full circuit for a stabilizer check, and real-time operations such as measurement and feed-forward [46]. While we have motivated mid-circuit measurement by its necessity in fault-tolerant quantum computing, many proposed near-term algorithms would benefit from this capability or the real-time operations it enables [47–50]. Thus, we expect the `mcm-rb` suite and developments upon it to also have immediate impact in characterizing devices for near-term applications.

## ACKNOWLEDGMENTS

The authors would like to thank Chris Wood for insightful discussions regarding numerical simulation with Qiskit Aer. The device was designed and fabricated internally at IBM. We acknowledge the use of IBM Quantum services for this work, and these results were enabled by the work of the IBM Quantum software and hardware teams. Access to devices was supported by IARPA under LogiQ (contract W911NF-16-1-0114). The research of this manuscript was sponsored by the Army Research Office and was accomplished under Grant Number W911NF-21-1-0002. The views and conclusions contained in this document are those of the authors and should not be interpreted as representing the official policies, either expressed or implied, of the Army Research Office or the U.S. Government. The U.S. Government is authorized to reproduce and distribute reprints for Government purposes notwithstanding any copyright notation herein.

## Appendix A: Experimental details

The mode of operation we employ to perform the `mcm-rb` suite simultaneously across `ibm_peekskill` is to parallelize both over control and ancilla qubits. We break the full set of qubits into groups that each consist of one ancilla qubit and two or three control qubits. As shown in Fig. 7, with just two configurations of 17 qubits each we can cover 23 of the 27 qubits on `ibm_peekskill`. For each protocol that involved Clifford RB, we used 40 random sequences for each of the 15 sequence lengths, and took 1024 shots for each sequence. Each configuration therefore consisted of 1800 circuits total, which was broken into 5 jobs that were run sequentially.

## Appendix B: Numerical simulation details

The Qiskit Aer simulator we employ is a gate-based simulator of a quantum circuit, with non-unitary noise channels implemented in Kraus form. To simulate the action of mid-circuit measurement, we apply a completely dephasing channel to the ancilla qubit,  $\mathcal{E}_m^a$ , which is described by the Kraus operators  $K_0 = |0\rangle\langle 0|$  and

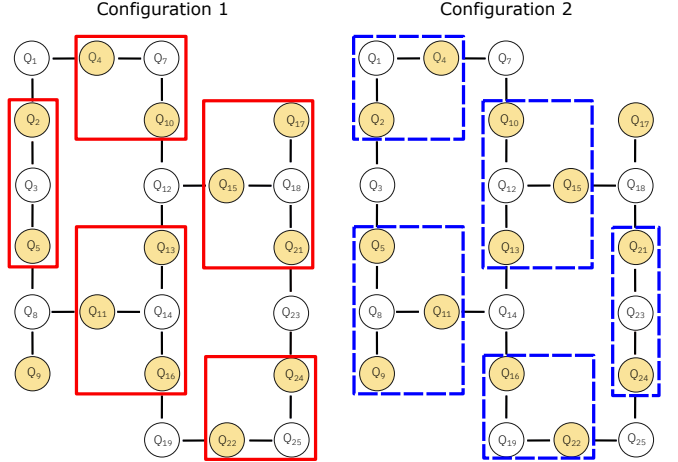


FIG. 7. Configurations for the two simultaneous `mcm-rb` suite experiments that each involved 17 qubits from `ibm_peekskill`. Ancilla qubits are shown in white, and control qubits in yellow. Red/blue squares encompass each ancilla-controls group.

$K_1 = |1\rangle\langle 1|$ . As we discard the outcomes of our mid-circuit measurements in experiment,  $\mathcal{E}_m^a$  is equivalent to the action of ideal mid-circuit measurement in the ensemble average.

To add errors to the mid-circuit measurement, we sandwich each application of  $\mathcal{E}_m^a$  with a pre-measurement and post-measurement two-qubit noise channel, which we label  $\mathcal{E}_{\text{pre}}$  and  $\mathcal{E}_{\text{post}}$ . Table II shows the choice of  $\mathcal{E}_{\text{pre}}$  and  $\mathcal{E}_{\text{post}}$  for each of our simulations. In addition to the errors before and after measurement, all single-qubit gates in our simulation have a depolarizing error channel ( $\eta = 10^{-3}$ ) applied after the action of the gate.

Simulation	$\mathcal{E}_{\text{pre}}$	$\mathcal{E}_{\text{post}}$
non-QND measurement	$\mathcal{E}_{T_1, T_2}^c$	$\mathcal{E}_{\text{dep}}^a$
Stark shift	$\hat{U}_{\text{Stark}}^c$	$\mathcal{E}_{T_1, T_2}^c$
Cross-measurement	$\mathcal{E}_{p_m}^c$	$\mathcal{E}_{T_1, T_2}^c$
Frequency collision	$\hat{U}_{\text{Col}}$	$\mathcal{E}_{T_1, T_2}^c$
ZZ-coupling	$\hat{U}_{\text{ZZ}}$	$\mathcal{E}_{T_1, T_2}^{a,c}$

TABLE II. Error channels used for each of our simulations.  $\mathcal{E}_{T_1, T_2}^c$  applies an identity channel to the ancilla, and a phase and amplitude damping channel to the control qubit equivalent to relaxation and dephasing with  $T_1 = 345 \mu\text{s}$ ,  $T_2 = 280 \mu\text{s}$ , and a duration  $t_m = 0.71 \mu\text{s}$ , which is meant to be representative of our experimental device.  $\mathcal{E}_{T_1, T_2}^{a,c}$  applies the same channel as  $\mathcal{E}_{T_1, T_2}^c$  to the control qubit, and a phase and amplitude damping channel to the ancilla qubit with varying  $T_1$  (see Fig. 6) and  $T_2 = T_1/3$ .  $\mathcal{E}_{\text{dep}}^a$  implements identity on the control and the depolarizing channel of Eq. (2) on the ancilla.  $\hat{U}_{\text{Stark}}^c$  and  $\mathcal{E}_{p_m}^c$  apply identity on the ancilla, while on the control applying the Stark-shift unitary  $Z$ -phase error and the cross-measurement error channel of Eq. (4), respectively.  $\hat{U}_{\text{Col}}$  implements the two-qubit unitary error of Eq. (4).

For simulations of `mcm-rb` we use 60 random Clifford sequences at each sequence length, and we sweep the er-

ror parameter of each model to generate the data points shown in the upper panels of the figures in section V. The calculation of the exact average gate infidelity,  $1 - \mathcal{F}$ , for the two single-qubit control error channels can be done analytically [51], and the expressions are

$$1 - \mathcal{F}_{\text{Stark}} = \frac{1}{3} (1 - \cos(2\phi)), \quad (\text{B1})$$

$$1 - \mathcal{F}_{\text{CM}} = \frac{p_m}{3}. \quad (\text{B2})$$

To calculate the average gate infidelity on the control qubit for the two-qubit collision error, we must first calculate the effective single-qubit channel this error induces on the control qubit. To do so, following the approach of [52], we first construct the Choi state of the two-qubit channel

$$\sigma_{\mathcal{U}_{\text{col}}} = \frac{1}{4} \sum_{j,k} |j\rangle\langle k| \otimes \mathcal{U}_{\text{col}} (|j\rangle\langle k|), \quad (\text{B3})$$

where  $\{|j\rangle\}$  is an orthonormal basis for the two-qubit Hilbert space and  $\mathcal{U}_{\text{col}}(\rho) = \hat{U}_{\text{col}}\rho\hat{U}_{\text{col}}^\dagger$  is the quantum channel representation of the unitary  $\hat{U}_{\text{col}}$ .

For a quantum channel  $\mathcal{E}$  that acts on the linear operator space of a Hilbert space  $\mathcal{H}$  the Choi state is constructed by acting with the channel  $\mathcal{I} \otimes \mathcal{E}$  on a maximally entangled state of the Hilbert space  $\mathcal{H} \otimes \mathcal{H}$ , where  $\mathcal{I}$  is the identity channel. In our case,  $\mathcal{H} \otimes \mathcal{H} = \mathcal{H}^a \otimes \mathcal{H}^c \otimes \mathcal{H}^a \otimes \mathcal{H}^c$ , where  $\mathcal{H}^{c/a}$  is the Hilbert space for the control/ancilla qubit. To calculate the effective channel on the control qubit alone, we perform a partial trace of  $\sigma_{\mathcal{U}_{\text{col}}}$  over the two copies of the ancilla Hilbert space

$$\sigma_{\mathcal{U}_{\text{col}}}^c = \frac{1}{4} \sum_{j,k} \text{Tr}_a [|j\rangle\langle k|] \otimes \text{Tr}_a [\mathcal{U}_{\text{col}} (|j\rangle\langle k|)]. \quad (\text{B4})$$

For each value of  $\Delta/J$  in Fig. 5 we perform this partial trace numerically to calculate the effective control qubit error channel Choi state, from which we can extract the average gate infidelity.

### Appendix C: Full mcm-rb suite data

The full set of mcm-rb suite decay curves for configuration 1 and configuration 2 on `ibm_peekskill` are shown in Fig. 8 and Fig. 9 respectively. For these plots, each row corresponds to a distinct ancilla-controls group shown in Fig. 7. Each column is one of the three protocols in the mcm-rb suite.

### Appendix D: Code and data availability

Experimental data, code for the numerical simulations, and Jupyter notebooks to reproduce the figures are available at <https://doi.org/10.5281/zenodo.6815663>.

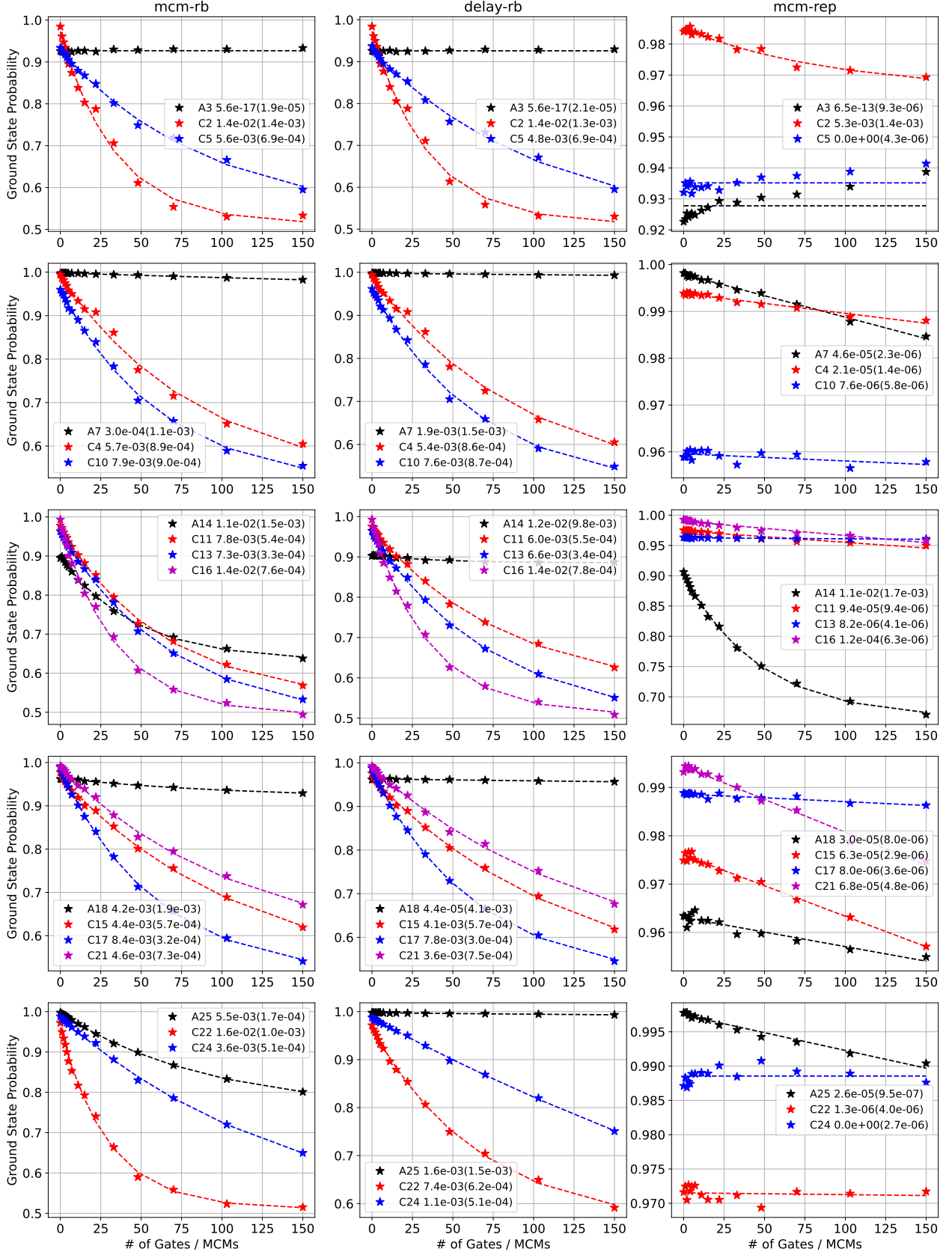


FIG. 8. The mcm-rb suite decay curves for the qubits studied in configuration 1 of Fig. 7 on `ibm_peekskill`. Each row corresponds to a distinct ancilla-controls group, and each column is one protocol from the mcm-rb suite.

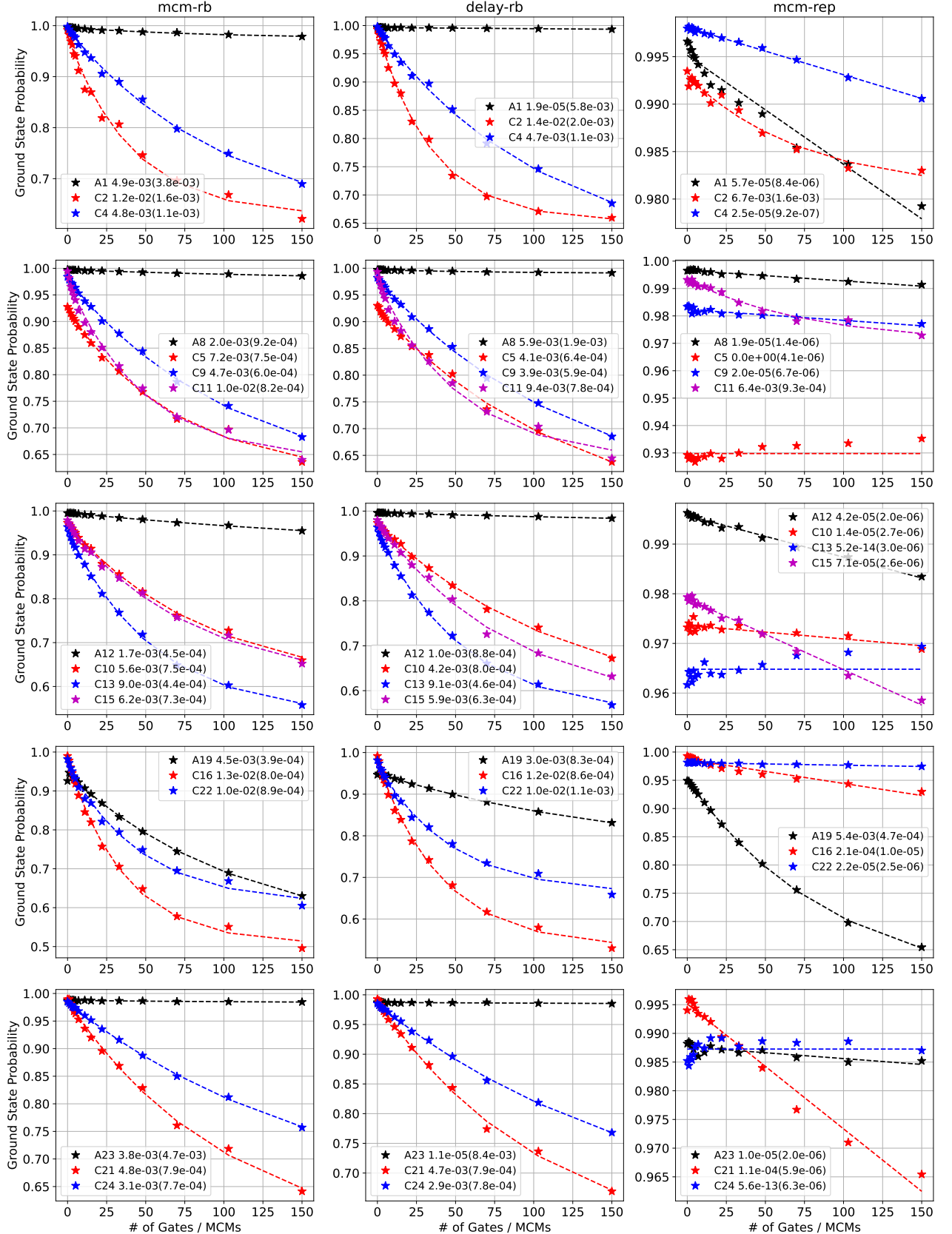


FIG. 9. The mcm-rb suite decay curves for the qubits studied in configuration 2 of Fig. 7 on `ibm_peekskill`. Each row corresponds to a distinct ancilla-controls group, and each column is one protocol from the mcm-rb suite.

---

[1] L. Egan, D. M. Debroy, C. Noel, A. Risinger, D. Zhu, D. Biswas, M. Newman, M. Li, K. R. Brown, M. Cetina, and C. Monroe, Fault-tolerant control of an error-corrected qubit, *Nature* **598**, 281 (2021).

[2] Z. Chen and Google Quantum AI, Exponential suppression of bit or phase errors with cyclic error correction, *Nature* **595**, 383 (2021).

[3] L. Postler, S. Heußen, I. Pogorelov, M. Rispler, T. Feldker, M. Meth, C. D. Marciniak, R. Stricker, M. Ringbauer, R. Blatt, P. Schindler, M. Müller, and T. Monz, Demonstration of fault-tolerant universal quantum gate operations, *Nature* **605**, 675 (2022).

[4] K. J. Satzinger and Google Quantum AI, Realizing topologically ordered states on a quantum processor, *Science* **374**, 1237 (2021).

[5] C. Ryan-Anderson, J. G. Bohnet, K. Lee, D. Gresh, A. Hankin, J. P. Gaebler, D. Francois, A. Chernoguzov, D. Lucchetti, N. C. Brown, T. M. Gatterman, S. K. Halit, K. Gilmore, J. A. Gerber, B. Neyenhuis, D. Hayes, and R. P. Stutz, Realization of real-time fault-tolerant quantum error correction, *Phys. Rev. X* **11**, 041058 (2021).

[6] M. H. Abobeih, Y. Wang, J. Randall, S. J. H. Loenen, C. E. Bradley, M. Markham, D. J. Twitchen, B. M. Terhal, and T. H. Taminiau, Fault-tolerant operation of a logical qubit in a diamond quantum processor, *Nature* **606**, 884 (2022).

[7] E. H. Chen, T. J. Yoder, Y. Kim, N. Sundaresan, S. Srinivasan, M. Li, A. D. Córcoles, A. W. Cross, and M. Takita, Calibrated decoders for experimental quantum error correction, *Phys. Rev. Lett.* **128**, 110504 (2022).

[8] S. Krinner, N. Lacroix, A. Remm, A. Di Paolo, E. Genois, C. Leroux, C. Hellings, S. Lazar, F. Swiadek, J. Herrmann, G. J. Norris, C. K. Andersen, M. Müller, A. Blais, C. Eichler, and A. Wallraff, Realizing repeated quantum error correction in a distance-three surface code, *Nature* **605**, 669 (2022).

[9] Y. Zhao, Y. Ye, H.-L. Huang, Y. Zhang, D. Wu, H. Guan, Q. Zhu, Z. Wei, T. He, S. Cao, F. Chen, T.-H. Chung, H. Deng, D. Fan, M. Gong, C. Guo, S. Guo, L. Han, N. Li, S. Li, Y. Li, F. Liang, J. Lin, H. Qian, H. Rong, H. Su, L. Sun, S. Wang, Y. Wu, Y. Xu, C. Ying, J. Yu, C. Zha, K. Zhang, Y.-H. Huo, C.-Y. Lu, C.-Z. Peng, X. Zhu, and J.-W. Pan, Realization of an error-correcting surface code with superconducting qubits (2021), arXiv:2112.13505.

[10] N. Sundaresan, T. J. Yoder, Y. Kim, M. Li, E. H. Chen, G. Harper, T. Thorbeck, A. W. Cross, A. D. Córcoles, and M. Takita, Matching and maximum likelihood decoding of a multi-round subsystem quantum error correction experiment (2022), arXiv:2203.07205.

[11] D. Ristè, M. Dukalski, C. A. Watson, G. de Lange, M. J. Tiggelman, Y. M. Blanter, K. W. Lehnert, R. N. Schouten, and L. DiCarlo, Deterministic entanglement of superconducting qubits by parity measurement and feedback, *Nature* **502**, 350 (2013).

[12] W. P. Livingston, M. S. Blok, E. Flurin, J. Dressel, A. N. Jordan, and I. Siddiqi, Experimental demonstration of continuous quantum error correction, *Nature Communications* **13**, 2307 (2022).

[13] A. Luis and L. L. Sánchez-Soto, Complete characterization of arbitrary quantum measurement processes, *Phys. Rev. Lett.* **83**, 3573 (1999).

[14] J. Fiurášek, Maximum-likelihood estimation of quantum measurement, *Phys. Rev. A* **64**, 024102 (2001).

[15] G. M. D'Ariano, L. Maccone, and P. L. Presti, Quantum calibration of measurement instrumentation, *Phys. Rev. Lett.* **93**, 250407 (2004).

[16] J. S. Lundeen, A. Feito, H. Coldenstrodt-Ronge, K. L. Pregnell, C. Silberhorn, T. C. Ralph, J. Eisert, M. B. Plenio, and I. A. Walmsley, Tomography of quantum detectors, *Nature Physics* **5**, 27 (2009).

[17] Y. Chen, M. Farahzad, S. Yoo, and T.-C. Wei, Detector tomography on ibm quantum computers and mitigation of an imperfect measurement, *Phys. Rev. A* **100**, 052315 (2019).

[18] K. Rudinger, G. J. Ribeill, L. C. G. Goria, M. Ware, E. Nielsen, K. Young, T. A. Ohki, R. Blume-Kohout, and T. Proctor, Characterizing midcircuit measurements on a superconducting qubit using gate set tomography, *Phys. Rev. Applied* **17**, 014014 (2022).

[19] L. Pereira, J. J. García-Ripoll, and T. Ramos, Complete physical characterization of quantum nondemolition measurements via tomography, *Phys. Rev. Lett.* **129**, 010402 (2022).

[20] L. Pereira, J. J. García-Ripoll, and T. Ramos, Parallel qnd measurement tomography of multi-qubit quantum devices (2022), arXiv:2204.10336.

[21] J. Helsen, I. Roth, E. Onorati, A. Werner, and J. Eisert, General framework for randomized benchmarking, *PRX Quantum* **3**, 020357 (2022).

[22] E. Knill, D. Leibfried, R. Reichle, J. Britton, R. B. Blakestad, J. D. Jost, C. Langer, R. Ozeri, S. Seidelin, and D. J. Wineland, Randomized benchmarking of quantum gates, *Phys. Rev. A* **77**, 012307 (2008).

[23] E. Magesan, J. M. Gambetta, and J. Emerson, Scalable and robust randomized benchmarking of quantum processes, *Phys. Rev. Lett.* **106**, 180504 (2011).

[24] E. Magesan, J. M. Gambetta, and J. Emerson, Characterizing quantum gates via randomized benchmarking, *Phys. Rev. A* **85**, 042311 (2012).

[25] E. Magesan, J. M. Gambetta, B. R. Johnson, C. A. Ryan, J. M. Chow, S. T. Merkel, M. P. da Silva, G. A. Keefe, M. B. Rothwell, T. A. Ohki, M. B. Ketchen, and M. Steffen, Efficient measurement of quantum gate error by interleaved randomized benchmarking, *Phys. Rev. Lett.* **109**, 080505 (2012).

[26] J. M. Gambetta, A. D. Córcoles, S. T. Merkel, B. R. Johnson, J. A. Smolin, J. M. Chow, C. A. Ryan, C. Rigetti, S. Poletto, T. A. Ohki, M. B. Ketchen, and M. Steffen, Characterization of addressability by simultaneous randomized benchmarking, *Phys. Rev. Lett.* **109**, 240504 (2012).

[27] J. Wallman, C. Granade, R. Harper, and S. T. Flammia, Estimating the coherence of noise, *New Journal of Physics* **17**, 113020 (2015).

[28] J. J. Wallman, M. Barnhill, and J. Emerson, Robust characterization of leakage errors, *New Journal of Physics* **18**, 043021 (2016).

[29] A. W. Cross, E. Magesan, L. S. Bishop, J. A. Smolin, and J. M. Gambetta, Scalable randomised benchmarking of non-clifford gates, *npj Quantum Information* **2**, 16012 (2016).

[30] C. J. Wood and J. M. Gambetta, Quantification and characterization of leakage errors, *Phys. Rev. A* **97**, 032306 (2018).

[31] D. C. McKay, S. Sheldon, J. A. Smolin, J. M. Chow, and J. M. Gambetta, Three-qubit randomized benchmarking, *Phys. Rev. Lett.* **122**, 200502 (2019).

[32] J. Helsen, X. Xue, L. M. K. Vandersypen, and S. Wehner, A new class of efficient randomized benchmarking protocols, *npj Quantum Information* **5**, 71 (2019).

[33] T. J. Proctor, A. Carignan-Dugas, K. Rudinger, E. Nielsen, R. Blume-Kohout, and K. Young, Direct randomized benchmarking for multiqubit devices, *Phys. Rev. Lett.* **123**, 030503 (2019).

[34] A. Erhard, J. J. Wallman, L. Postler, M. Meth, R. Stricker, E. A. Martinez, P. Schindler, T. Monz, J. Emerson, and R. Blatt, Characterizing large-scale quantum computers via cycle benchmarking, *Nature Communications* **10**, 5347 (2019).

[35] D. C. McKay, A. W. Cross, C. J. Wood, and J. M. Gambetta, Correlated randomized benchmarking (2020), arXiv:2003.02354.

[36] T. Proctor, S. Seritan, K. Rudinger, E. Nielsen, R. Blume-Kohout, and K. Young, Scalable randomized benchmarking of quantum computers using mirror circuits (2021), arXiv:2112.09853.

[37] A. Morvan, V. V. Ramasesh, M. S. Blok, J. M. Kreikebaum, K. O'Brien, L. Chen, B. K. Mitchell, R. K. Naik, D. I. Santiago, and I. Siddiqi, Qutrit randomized benchmarking, *Phys. Rev. Lett.* **126**, 210504 (2021).

[38] J. P. Gaebler, C. H. Baldwin, S. A. Moses, J. M. Dreiling, C. Figgatt, M. Foss-Feig, D. Hayes, and J. M. Pino, Suppression of midcircuit measurement crosstalk errors with micromotion, *Phys. Rev. A* **104**, 062440 (2021).

[39] V. B. Braginsky, Y. I. Vorontsov, and K. S. Thorne, Quantum nondemolition measurements, *Science* **209**, 547 (1980).

[40] J. Gambetta, A. Blais, D. I. Schuster, A. Wallraff, L. Frunzio, J. Majer, M. H. Devoret, S. M. Girvin, and R. J. Schoelkopf, Qubit-photon interactions in a cavity: Measurement-induced dephasing and number splitting, *Phys. Rev. A* **74**, 042318 (2006).

[41] L. C. G. Govia and F. K. Wilhelm, Unitary-feedback-improved qubit initialization in the dispersive regime, *Phys. Rev. Applied* **4**, 054001 (2015).

[42] J. C. Pommerening and D. P. DiVincenzo, What is measured when a qubit measurement is performed on a multiqubit chip, *Phys. Rev. A* **102**, 032623 (2020).

[43] K. Rudinger, C. W. Hogle, R. K. Naik, A. Hashim, D. Lobser, D. I. Santiago, M. D. Grace, E. Nielsen, T. Proctor, S. Seritan, S. M. Clark, R. Blume-Kohout, I. Siddiqi, and K. C. Young, Experimental characterization of crosstalk errors with simultaneous gate set tomography, *PRX Quantum* **2**, 040338 (2021).

[44] Qiskit: An open-source framework for quantum computing (2021).

[45] H. Ball, T. M. Stace, S. T. Flammia, and M. J. Biercuk, Effect of noise correlations on randomized benchmarking, *Phys. Rev. A* **93**, 022303 (2016).

[46] D. Ristè, L. C. G. Govia, B. Donovan, S. D. Fallek, W. D. Kalfus, M. Brink, N. T. Bronn, and T. A. Ohki, Real-time processing of stabilizer measurements in a bit-flip code, *npj Quantum Information* **6**, 71 (2020).

[47] M. Urbanek, B. Nachman, and W. A. de Jong, Error detection on quantum computers improving the accuracy of chemical calculations, *Phys. Rev. A* **102**, 022427 (2020).

[48] A. D. Córcoles, M. Takita, K. Inoue, S. Lekuch, Z. K. Minev, J. M. Chow, and J. M. Gambetta, Exploiting dynamic quantum circuits in a quantum algorithm with superconducting qubits, *Phys. Rev. Lett.* **127**, 100501 (2021).

[49] L. Botelho, A. Glos, A. Kundu, J. A. Miszczak, O. Salehi, and Z. Zimborás, Error mitigation for variational quantum algorithms through mid-circuit measurements, *Phys. Rev. A* **105**, 022441 (2022).

[50] C. Piveteau and D. Sutter, Circuit knitting with classical communication (2022), arXiv:2205.00016.

[51] J. Emerson, R. Alicki, and K. Życzkowski, Scalable noise estimation with random unitary operators, *Journal of Optics B: Quantum and Semiclassical Optics* **7**, S347 (2005).

[52] L. C. G. Govia, G. J. Ribeill, D. Ristè, M. Ware, and H. Krovi, Bootstrapping quantum process tomography via a perturbative ansatz, *Nature Communications* **11**, 1084 (2020).